Iraqi Journal of Physics, 2018 *Vol.16, No.38, PP. 83-98*
DOI: 10.20723/ijp.16.38.83-98

The emission spectra and hydrodynamic properties of Al plasma using Nd-YAG laser

Shaymaa N. Ayyash and Mahmoad SH. Mahmoad

Institute of Laser for Postgraduate Studies, University of Baghdad, Baghdad, Iraq

E-mail: Mahm823@yahoo.com

Abstract

In this work, the emission spectra and atomic structure of the aluminum target had been studied theoretically using Cowan code. Cowan code was used to calculate the transitions of electrons between atomic configuration interactions using the mathematical method called (Hartree-Fock). The aluminum target can give a good emission spectrum in the XUV region at 10 nm with oscillator strength of 1.82.

The hydrodynamic properties of laser produced plasma (LPP) were investigated for the purpose of creating a light source working in the EUV region. Such a light source is very important for lithography (semiconductor manufacturing). The improved MEDUSA (Med103) code can calculate the plasma hydrodynamic properties (velocity, electron density, pressure, electron temperature, ion density, ion temperature and average ionization Z*). Aluminum target was considered in these calculations (Z=13). This work was done by using three laser power densities (10^{11}, 10^{12} and 10^{13} W/cm^2) with a 10 ns pulse width and 10 ps pulse width for laser wavelength (1064 nm). These laser intensities with 10 ns pulse width give high ionization stage of the Aluminum from 2.4-11 for electron range from 16.5-3000 eV.

Key words
Hydrodynamic properties, emission spectra, Cowan code, Nd-YAG laser, medusa code.

Article info.
Received: Feb. 2018
Accepted: Apr. 2018
Published: Sep. 2018

أطياف الأنبعاث والخواص الهيدرودينميكية لبلازما الألمنيوم بأستخدام ليزر النيديميوم-ياك

شيماء نعمه عياش و محمود شاكر محمود

معهد الليزر للدراسات العليا، جامعة بغداد، بغداد، العراق

الخلاصة

في هذا العمل. تمت دراسة أطياف الانبعاث والتركيب الذري للألمنيوم نظريا بأستخدام برنامج المحاكاة (Cowan code). تم استخدام برنامج (Cowan) في المحاكاة النظرية لحساب الأنتقالات الألكترونية بين التوزيعات الذرية بأستعمال طريقة (Hartree Fock) الرياضية. ان الألمنيوم اعطي طيف انبعاثي جيد في منطقة فوق البنفسجية البعيده عند الطول الموجي 10 نانومتر مع قوة انتقال 1.82.

تمت دراسة الخصائص الهيدرودينميكيه للبلازما المتولدة بالليزر لغرض الحصول على مصدر ضوئي ضمن منطقة الاشعة فوق البنفسجية البعيدة. أن هذا المصدر الضوئي مهم جدا في عملية الطباعة النقشية والتي تستخدم في صناعة اشباه الموصلات. تم استعمال البرنامج المطور لبرنامج (Medusa) الأصلي والمسمى Med103 ايضا والذي يدرس خصائص البلازما المنتجه بالليزر ضمن بعد هيدرودينميكي واحد.ان برنامج (Med103) المطور يحسب الخصائص الهيدرودينيميكية للبلازما مثل (السرعة، كثافة الألكترون، الضغط، درجة حرارة الألكترون، كثافة الأيون، درجة حرارة الأيون ومعدل الأيونات) .تمت دراسة هذه الصفات بأستخدام ثلاثة قيم مختلفه لكثافة قدرة الليزر (10^{11}, 10^{12}, 10^{13} واط/سم^3) وكان عرض النبضة الليزرية المستخدمة هو (10 نانوثانية و 10 بيكوثانية) لليزر ذو الطول الموجي 1064 نانومتر. ان هذه القيم المختلفة لكثافة الليزر مع عرض النبضه 10 نانومتر اعطى معدل تأين عالي للألمنيوم من (2.4 – 11) لدرجة حرارة الالكترون من (16.5-3000) الكترون-فولت.

Introduction

There are four specific features that characterizing the laser produced plasma, which are [1]:

1- High temperature (up to 100 eV).
2- High density (electron density ≈ $10^{18} – 10^{21}$ cm^{-3}).
3- Relatively high degree of ionization.
4- High expansion velocities.

when the laser radiation first reaches the target, the penetration can happen for only a very short depth. This initial interaction occurs only for a very thin layer close to the target surface which is referred to as the skin depth, $\boldsymbol{\delta}$, where [2]

$$\boldsymbol{\delta} = (\boldsymbol{\upsilon}\, \boldsymbol{\mu}_o\, \boldsymbol{\sigma})^{-1/2} \qquad (1)$$

where $\boldsymbol{\upsilon}$ is the frequency of the incident radiation, $\boldsymbol{\sigma}$ is the conductivity of target and $\boldsymbol{\mu}_o$ is the permeability of the vacuum.

In vacuum, the maximum electric and magnetic fields (E_{max} and B_{max}) of the laser are related to the irradiance, $I_{L,}$ by [3]:

$$E_{max}\ (V/cm) \cong 2.75 \times 10^9\ (I_L\ /10^{16}\ (W/cm^2))^{1/2} \qquad (2)$$

$$B_{max}\ (Gauss) \cong 9.2 \times 10^6\ (I_L\ /10^{16}\ (W/cm^2))^{1/2} \qquad (3)$$

When the high power laser hitting the material, the plasma is created. The plasma expands rapidly in vacuum due to the large density gradient. The plasma is said to be isothermal according to the duration of the laser pulse.

In this case, the dynamic equilibrium is happened between the plasma absorption coefficient and the rapid transfer of thermal energy to kinetic energy [4].

The plasma largest acceleration is in the direction of smallest dimension, because of the larger pressure gradient, so that the expansion velocity along the target normal will be significantly larger than its perpendicular component. The calculations of numerical hydrodynamic are important to calculate the spatial and temporal velocity, temperature, pressure and ion distribution in laser produced plasma. In the steady state of this operation, emission depends on the ion stages. The spectral intensity and line shape will be effected by time-dependent hydrodynamics. In laser produced plasma, the spatial and temporal hydrodynamics are calculated by using the laser-matter interaction program Med103 (which is improved from MEDUSA code). A Fortran LPP code Med103, which is an updated version of MEDUSA code was used to model Plasma hydrodynamics. MEDUSA code was created by Christiansen in 1974 for the UKAEA group at Culham laboratory and it was designed to the simulation of inertial confinement fusion [5, 6].

New equations of state as an option to 'Medusa', based on the Thomas-Fermi model in 1980. Another addition was made in 1983, in which radiation transport by X-ray photon was added for comparison with spectroscopic results, with the details of line shape and line intensity ratio.
[7, 8].

Theoretical methods

For atomic system with N-electron, the non-relativistic Hamiltonian consists of the total kinetic energy of the N electrons plus the total potential energy according to their interaction with the nucleus and with each other.
The Hamiltonian equation is:

$$H=\sum_{i=1}^{N}\left(-\frac{1}{2}\nabla_i^2-\frac{Z}{r_i}\right)+\sum_{i>j}\frac{1}{r_{ij}} \qquad (4)$$

where z is the charge, r_i is the distance from electron (i) to the nucleus and r_{ij}

is the distance between the electron (i) and the electron (j).

The Hartree-Fock method is a non-relativistic method and in general several relativistic corrections are made to the non-relativistic Hamiltonian to provide for more accurate results. The Dirac equation, a fully relativistic method of calculating atomic structure with an equivalent scheme of coupled integro-differential equations is one which is based on the relativistic equation for the electron. Such scheme, which is similar to Hartree-Fock scheme in formulation, is known as the Dirac-Fock method. Configuration calculation interactions can also be performed using Slater determinants with the Dirac-Fock method. The corresponding generalization of the MCHF method is called the multiconfiguration Dirac-Fock (MCDF) method [9, 10].

Cowan code is the most widely available numerical computer code for calculating atomic structure. This fortran code was comprised by Robert D. Cowan in 1968 [11]. Based on Hartree-Fock equations, Cowan code is also employs several other approximations such as Hartree-Fock with exchange in which different methods are used for self-interaction correction and another method to approximate the remainder of the Hartree-Fock exchange term [12].

Medusa is a Fortran code which calculates the 1-dimensional hydrodynamic and thermodynamic behavior of a plasma irradiated by an intense laser beam. The results are intended to assist in understanding the ICF (inertial confinement fusion). This code was created by J. P. Christiansen et al. in 1974 at Culham Laboratory in UK [5]. Version 1 of Medusa is describing the plasma by four dependent variables. These variables are density (ρ), velocity (υ), ion temperature (T_i) and electron temperature (T_e). These are functions of the time (t) and of a single space variable (r) which can be chosen to correspond to slab, cylindrical or spherical geometry as required [5]. Navier - Stokes hydrodynamics equations are supplemented by separate heat conduction equations to calculate T_i and T_e. Many features have been added to Medusa code over many years and the code was named Med101 in 1989 and later on Med103 in 1996 [13].

In Medusa code, the plasma is assumed to consist of a charged-neutral mixture of electrons and various species of ions and atoms or molecules.The instantaneous local chemical composition can be described by a set of fractions f_k so that [14]

$$n_k = f_k n_i \qquad (5)$$

is the number density of ion of species *k*, where

$$\sum_k f_k = 1 \qquad (6)$$

The average mass and charge numbers associated with each ion can be given by

$$M = \sum_k f_k M_k \qquad (7)$$

$$Z = \sum_k f_k Z_k \qquad (8)$$

where M_k and Z_k are the mass and charge numbers of the individual species. The electron and ion densities are

$$n_e = Z\, n_i \quad (m^{-3}) \qquad (9)$$

and the physical density is

$$\rho = n_i\, M\, m_H = \frac{1}{V} \quad (kg / m^{-3}) \qquad (10)$$

The thermal conduction term is [15]

$$H = \frac{1}{\rho} \nabla . \dot{k} \nabla T \qquad (11)$$

where $\dot{k}$ is the thermal conductivity.

In Eq. (11), a limit is imposed on the electron thermal flux ($F_e = k_e \nabla T_e$), so called free-streaming limit

$$(F_e)_{max} = a\frac{1}{4} n_e v_e k T_e \ (W/m^2) \qquad (12)$$

where (a) is an adjustable numerical constant. The absorption is assumed to occur via inverse bremsstrahlung at densities below the critical density. The absorption coefficient is given by

$$\alpha = 13.51\lambda\text{-}2\beta^2(1-\beta)^{1/2}T_e^{-\frac{3}{2}} \times (5.05 + log\lambda\, T_e)Z^2 \qquad (13)$$

Result and discusses

Fig. 1 is a plot explains oscillator strength (*gf*) as a function of wavelength for different transitions for (AlII) ion computed by using Cowan code. This figure represents the emission spectrum for AlII (Mg like) ion. There is one emission range lying in 95.00 nm. The results and discussion adopted is in the nanometer scale as it is nowadays the standard for wavelength. The maximum oscillator strength in this range is 0.058 at λ = 95.00 nm. The second ionization stage (ALIII) emission oscillator strengths are represented in Fig. 2. The ALIII (Na like) is emitting a spectrum with oscillator strength of 0.135 at λ = 16.05 nm.

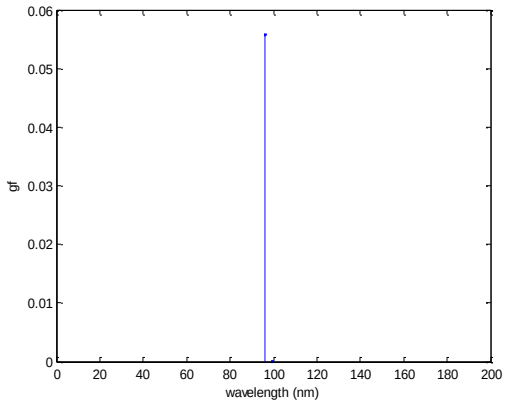

Fig. 1: Emission spectrum of the first ionization of (AlII).

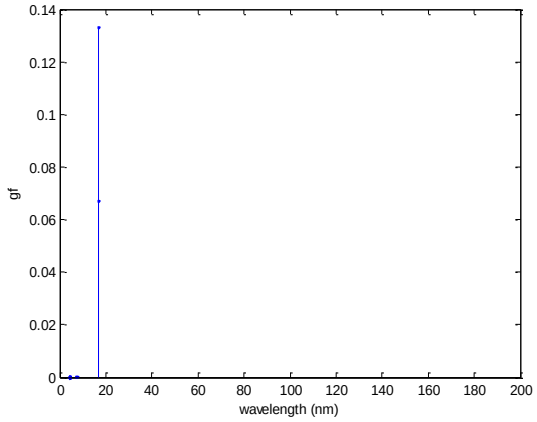

Fig. 2: Emission spectrum of the second ionization of (AlIII).

Fig. 3 represents the emission spectrum for Al IV (Ne like) ion which covers a wide range. The strongest transition at λ =127.50 nm with oscillator strength of 4.25, and the minimum emission spectrum with small oscillator strength is 0.10 at λ =140.20 nm. From this result the emission spectrum range can cover a wide range here that means the

decrease of the ionization number leads to increase the emission spectrum wavelength, this because of coulomb forces. The emission wavelength spectrum decreases as the number of electrons releases from the Aluminum atom increases. The AlV (F like) emission spectrum is shown in Fig. 4 where the maximum emission spectrum is at λ = 10 nm with strongest oscillator strength of 1.82.

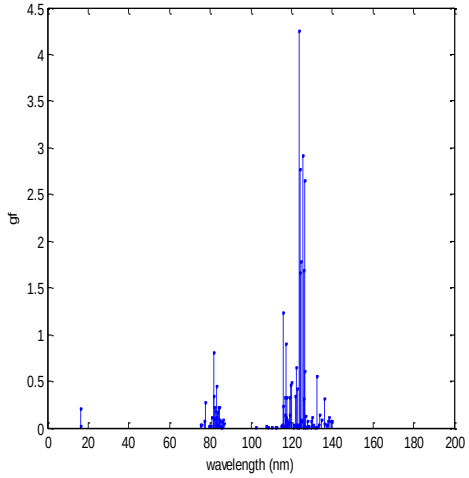

Fig. 3: Emission spectrum of the third ionization of (AlIV).

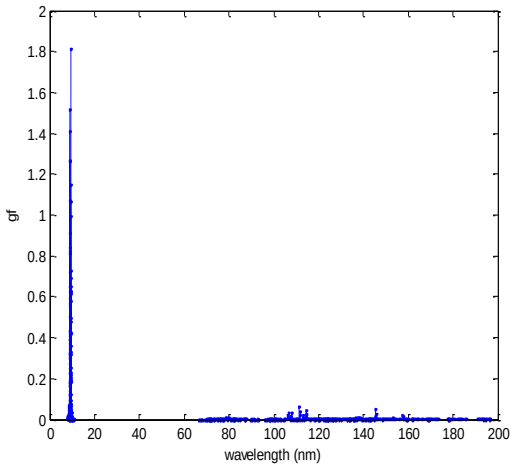

Fig. 4: Emission spectrum of the fourth ionization of (AlV).

The emission spectrum for the fifth ionization stage of AlVI (O like) is shown in Fig. 5. The highest oscillator strength is 3.25 and λ = 117.50 nm.

The emission wavelength here is covering a wide range from different transitions. The minimum emission spectrum is at λ= 200 nm of oscillator strength of 0.05. Fig. 6 describes the emission spectra for Al VI (N like) ion with a maximum emission wavelength of 115.50 nm with oscillator strength of 2.18. The minimum wavelength is 185.85 nm with oscillator strength of 0.05. In this form, there are thousands of lines in a very narrow region like oscillator strength of 1.85 with wavelength is 117.85 nm, emission spectrum at λ =112.25 nm with oscillator strength of 1.20, and emission spectrum with oscillator strength of 0.45 and λ =140.00 nm.

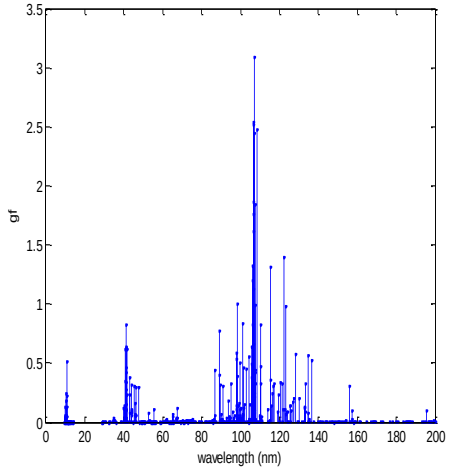

Fig. 5: Emission spectrum of the fifth ionization of (AlVI).

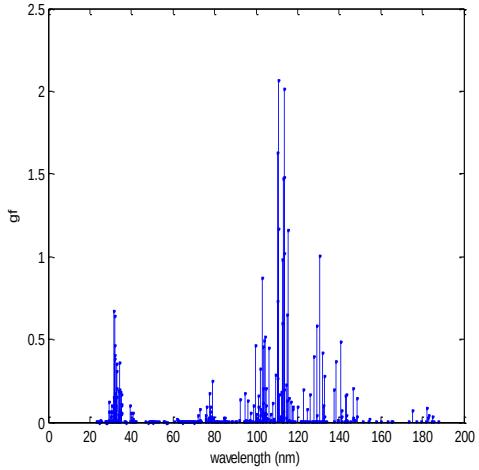

Fig. 6: Emission spectrum of the sixth ionization of (AlVII).

Fig. 7 shows the AlVIII (C like) ion oscillator strength behavior with a maximum emission spectrum at λ= 127.50 nm and oscillator strength of 1.25. In this form, there are many lines from emission spectrum transitions like these oscillator strength of 0.88 with wavelength of 132.25 nm, and λ = 153.50 nm with oscillator strength of 0.58, and oscillator strength of 0.15 and λ = 182.00 nm. Fig. 8 describes the emission spectra for AlIX (Be like) ion at a maximum emission wavelength of 320 nm with oscillator strength 3.18, but in the extreme ultraviolet region the maximum wavelength is 125.85nm with oscillator strength of 2.20.

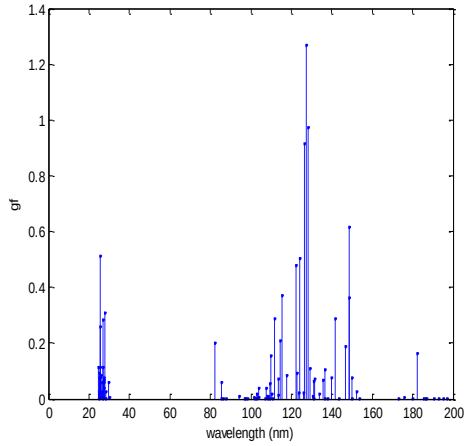

Fig. 7: Emission spectrum of the seventh ionization of (AlVIII).

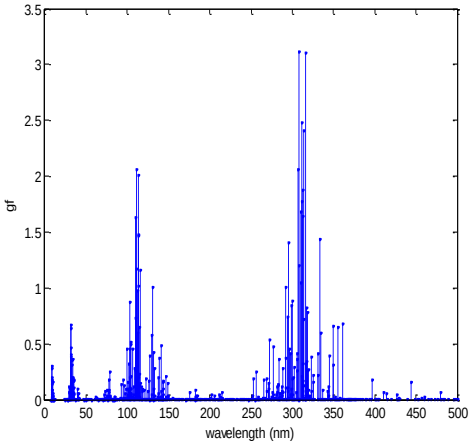

Fig. 8: Emission spectrum of the eighth ionization of (AlIX).

The AlX (B like) ion gives a maximum oscillator strength of 0.85 at λ= 1720.25 nm (Fig. 9). The minimum emission wavelength is at λ = 2000.30 nm with oscillator strength of 0.03. In this figure, there is another emission spectrum line near from strongest transition has a wavelength about 1450.00 nm with oscillator strength of 0.83. The maximum oscillator strength in the extreme ultraviolet radiation is 0.49 at λ =198 nm. The emission spectrum for the tenth ionization stage of AlXI (Li like) is presented in Fig. 10. The highest oscillator strength is 3.7 at λ =112 nm. The emission spectrum here is covering a wide range from different transitions. The minimum emission spectrum is at λ= 152.25 nm with oscillator strength of 0.02.

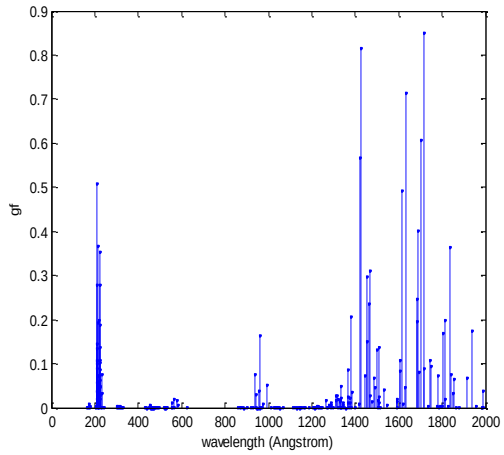

Fig. 9: Emission spectrum of the ninth ionization of (AlX).

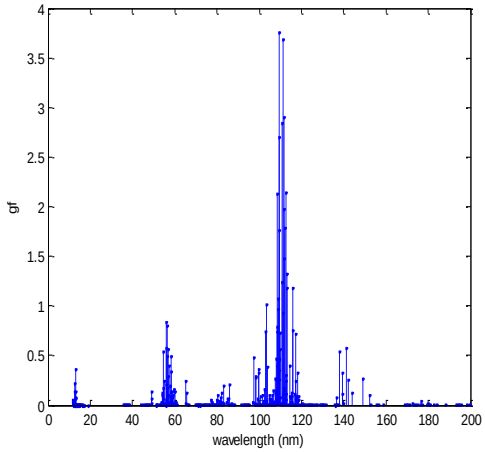

Fig. 10: Emission spectrum of the tenth ionization of (AlXI).

Medusa was developed to study the plasma parameters. The Aluminum planar shape target was proposed and an Nd: YAG laser beam with power densities 10^{11}, 10^{12}, and 10^{13} W/cm^2 are used.

Spatial and temporal electron density variation

Fig. 11 (a and b) describes the behavior of electron density as a function of space and time when the laser power density is 10^{11}W/cm^2 and pulse width is 10 ns. The plasma electron density begins from far the critical density (10^{23} cm^{-3}) then a strong drop happens to the electron density. When the laser power density increases to 10^{12} W/cm^2 was shown in Fig. 12(a), the electron density begins from far critical density of the plasma and strong drop to over than 10^{21} cm^{-3} at 85 µm. The electron density with the temporal variation of the plasma (Fig. 12(b)) shows that the maximum electron density is 10^{23} cm^{-3} at the beginning and decreases rapidly with the time. The decrease in temporal electron density of the plasma is relatively linear until 10 ns.

The effect of the 10 ps laser on the electron density profile was shown in Fig. 13(a) for 10^{11} W/cm^2 laser power density. The electron density begins from higher than 10^{23} cm^{-3} and drop to less than 10^{22} cm^{-3}. Fig.13(b) describes the electron density begins from 10^{23} cm^{-3} and decreases to 10^{20} cm^{-3} at 10 ns. The electron density obtained from the 10 nanosecond laser pulse width is more than that obtained from the 10 picosecond laser pulse width.

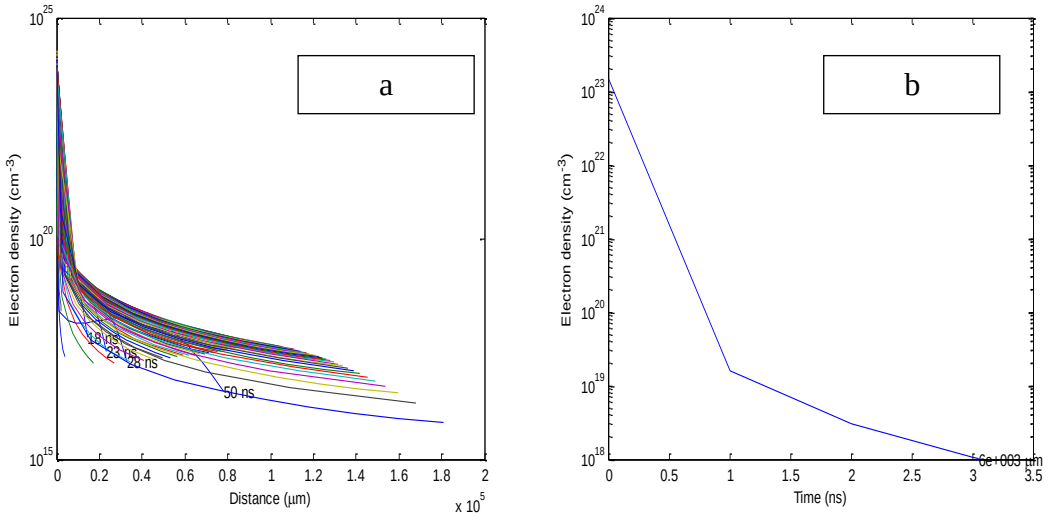

Fig. 11: Spatial and temporal variation of electron density at intensity 10^{11} W/cm^2 with pulse width 10 ns.

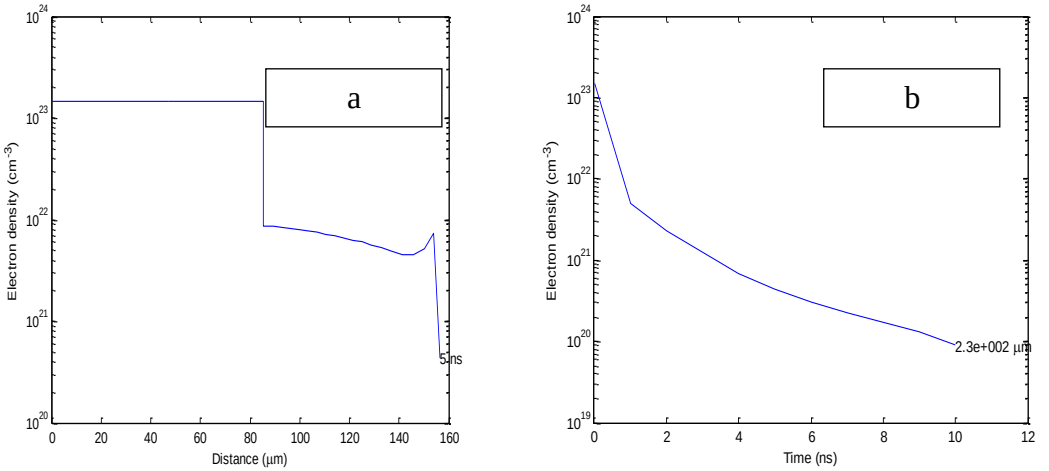

Fig. 12: Spatial and temporal variation of electron density at intensity 10^{12} W/cm^2 with pulse width 10 ns.

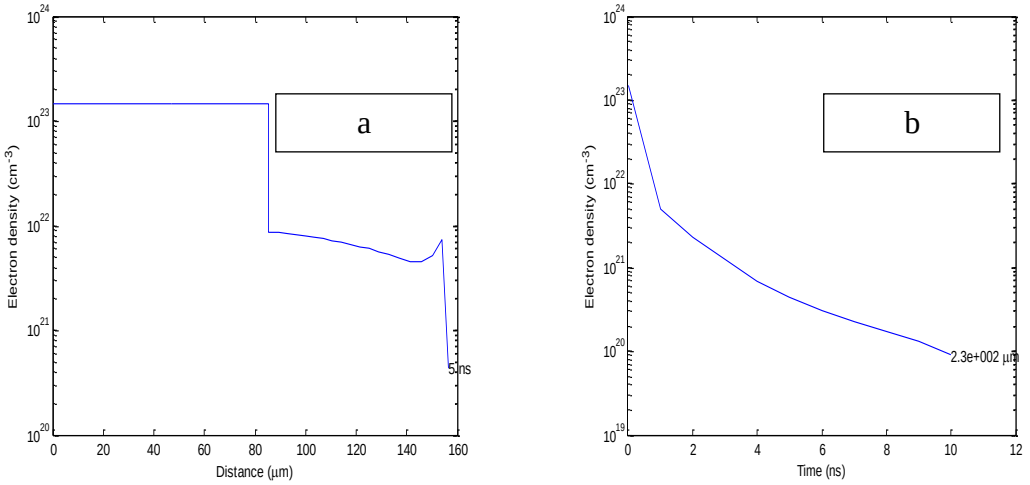

Fig. 13: Spatial and temporal variation of electron density at intensity 10^{11} W/cm^2 with pulse width 10 ps.

When the laser power density increases to 10^{12} W/cm^2 (Fig. 14(a and b), the maximum electron density is higher than 10^{23} cm^{-3} at 98 µm and then decreases gradually to reach 10^{19} cm^{-3} at 10 ns at a distance is about 1200 µm. Fig. 15(a) describes the relationship between the electron density and the time. The electron density begins from far critical density 10^{23} cm^{-3} and then decreases to more than 10^{18}cm^{-3}. Fig. 15(b) describes the relationship between the electron density and the time. The electron density begins from far critical density 10^{23} cm^{-3} and then decreases to more than 10^{18}cm^{-3} at 10 ns.

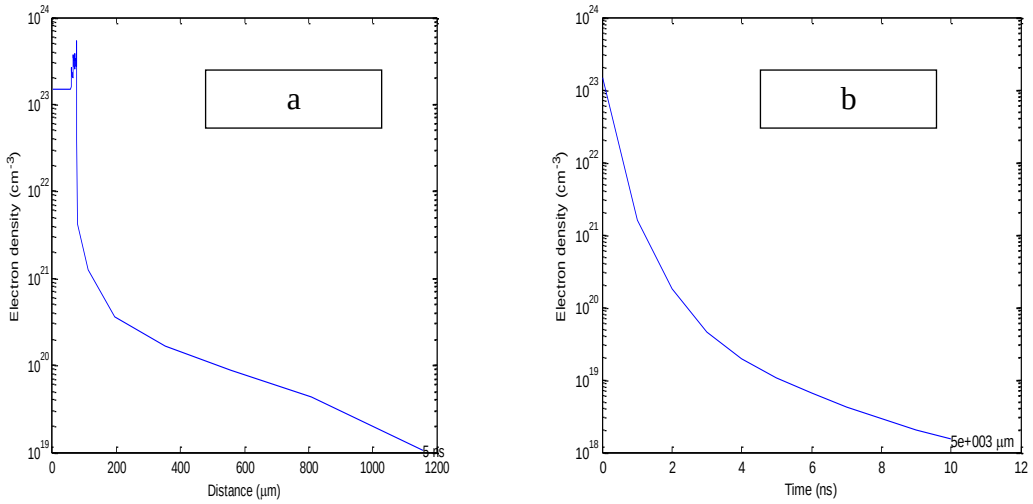

Fig. 14: Spatial and temporal variation of electron density at intensity 10^{12} W/cm^2 with pulse width 10 ps.

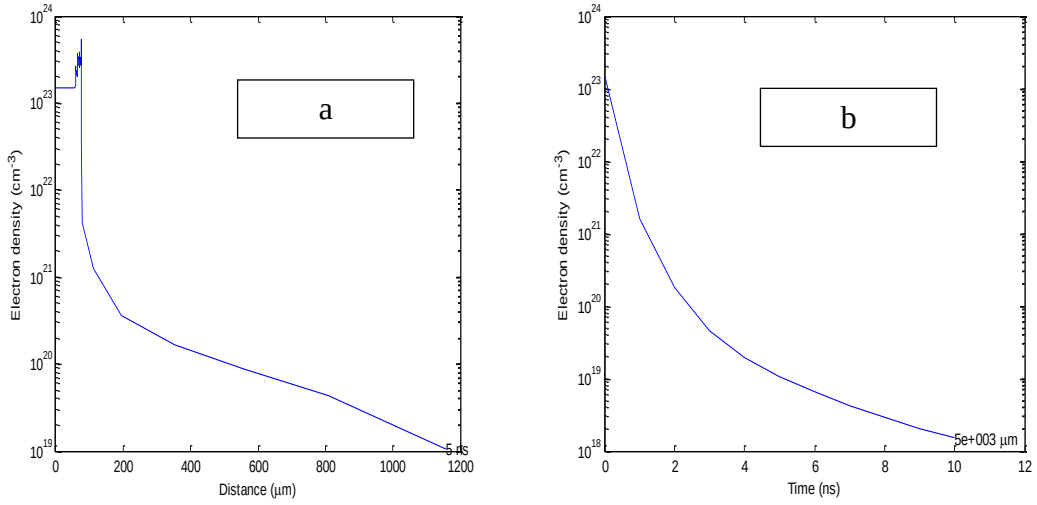

Fig. 15: Spatial and temporal variation of electron density at intensity 10^{13} W/cm^2 with pulse width 10 ps.

Spatial and temporal electron temperature variation

The electron temperature is a function of the laser power density, and it is one of the parameters of the plasma. Fig.16(a) represents the spatial variation of the plasma electron temperature when the laser power density is 10^{11} W/cm^2 and the pulse width is 10 ns. The peak of the electron temperature is 3000 eV after 2000 µm distance.

The temporal variation of the plasma electron temperature was shown in Fig.16(b). The plasma electron temperature begins from zero and increases reaching to 12.5 eV at about 4 ns, and then increases rapidly to reach 56 eV at 9.5 ns. Fig.17(a) explains the spatial variation of the plasma electron temperature when the laser power density increases to 10^{12} W/cm^2. The electron temperature after 150 µm distance increases reaching to 17 eV. The temporal variation of the plasma electron temperature was shown in Fig.17(b), the plasma electron temperature begins from zero and increases to 13 eV at 4 ns, and then increases to reach 85 eV after 9 ns. The spatial variation of the plasma electron temperature when the laser power density is 10^{11} W/cm^2 and pulse width is 10 ps was shown in Fig.18(a). The plasma electron temperature after 150 µm increases reaching to 16.5 eV. The temporal variation of the plasma electron temperature was shown in Fig.18(b). The electron temperature begins from zero and increases reaching to 13 eV at 4 ns, and then increases to reach 84 eV at 9.5 ns.

Fig.19(a) describes the spatial variation of the plasma electron temperature when the laser power density is 10^{12} W/cm^2 and pulse width is 10 ps. The plasma electron temperature increases to reach 900 eV after 80 µm, and then decreases rapidly to reach 750 eV at 1800 µm. Fig.19(b) represents the temporal variation of the plasma electron temperature when the laser power density is 10^{12} W/cm^2. The plasma electron temperature begins from zero and increases to reach 350 eV at 2 ns, and then increases reaching to 1900 eV after 9.5 ns.

The spatial variation of the plasma electron temperature when the laser power density is 10^{13} W/cm^2 and pulse width 10 ps was shown in Fig.20(a). The maximum plasma electron temperature is 950 eV at 240 µm and then decreases to 750 eV at 1180 µm. Fig.20(b) represents the temporal variation of the plasma when the laser power density is 10^{13} W/cm^2. The electron temperature begins from zero to 280 eV at 2 ns, and increases reaching to 1950 eV at 9.5 ns. From these results, when the laser power density increases, the plasma electron temperature also increases.

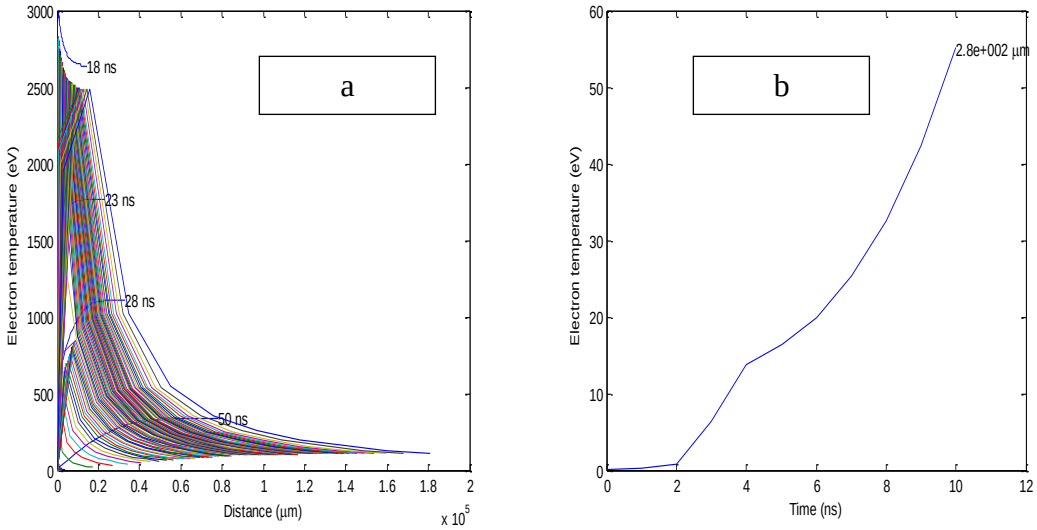

Fig. 16: Spatial and temporal variation of plasma electron temperature at intensity 10^{11} W/cm^2 with pulse width 10 ns.

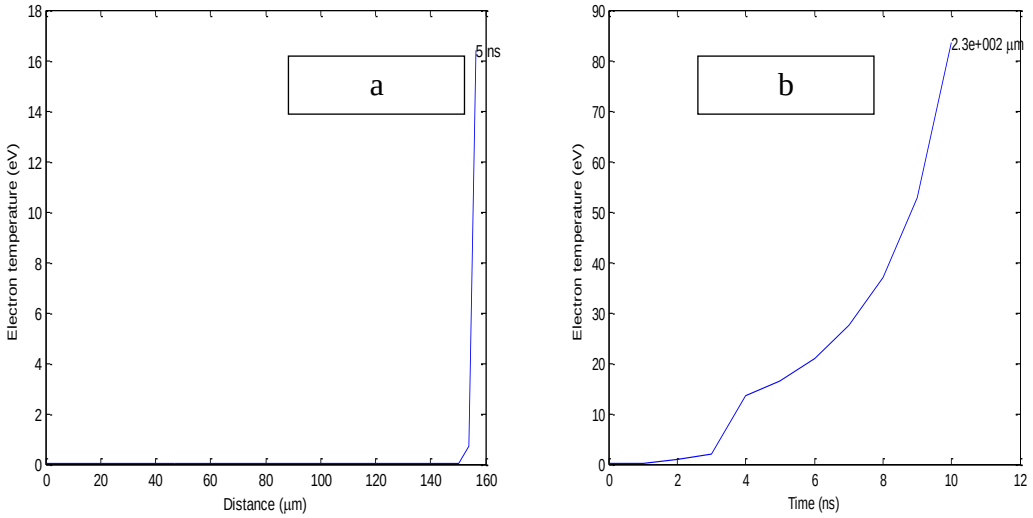

Fig. 17: Spatial and temporal variation of plasma electron temperature at intensity 10^{12} W/cm^2 with pulse width 10 ns.

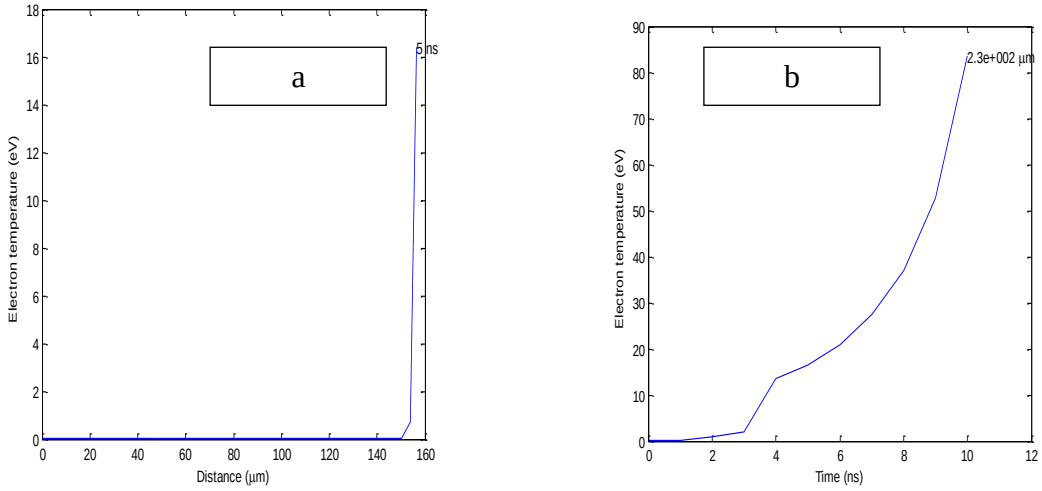

Fig. 18: Spatial and temporal variation of plasma electron temperature at intensity 10^{11} W/cm^2 with pulse width 10 ps.

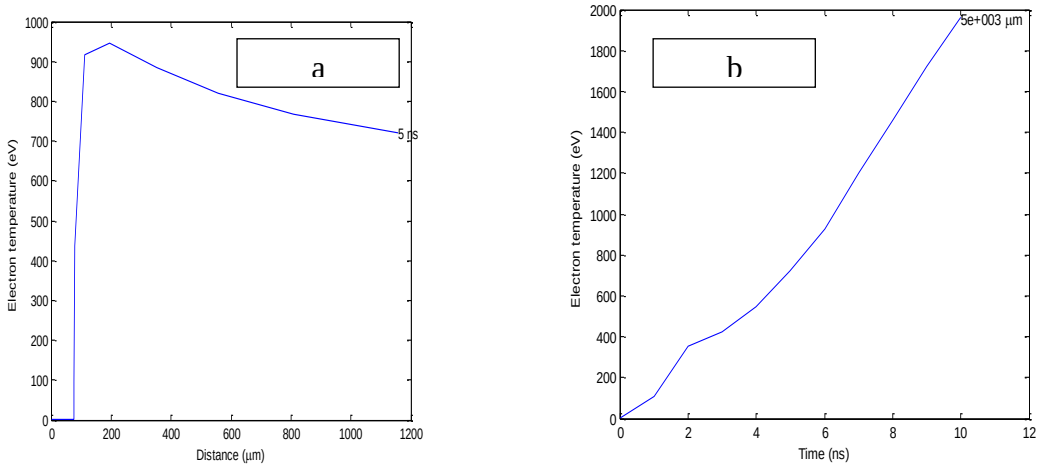

Fig. 19: Spatial and temporal variation of plasma electron temperature at intensity 10^{12} W/cm^2 with pulse width 10 ps.

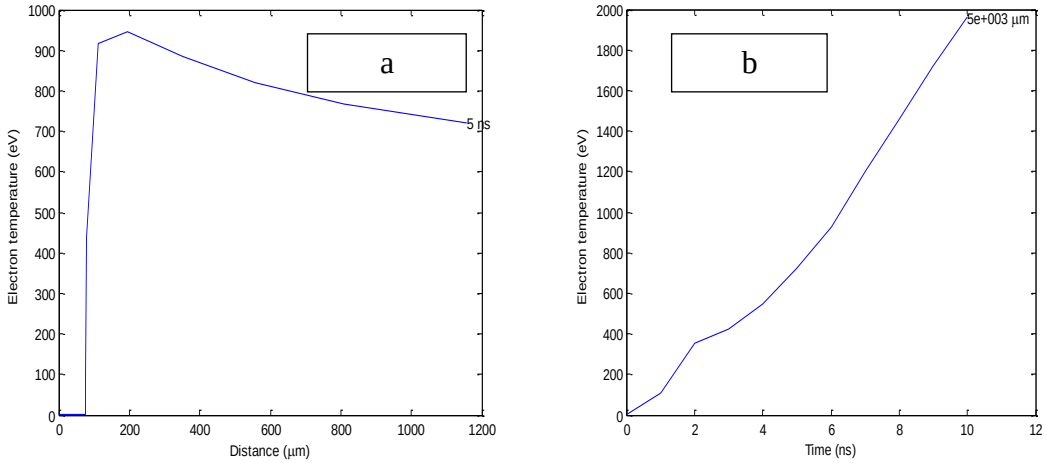

Fig. 20: Spatial and temporal variation of plasma electron temperature at intensity 10^{13} W/cm^2 with pulse width 10 ps.

Spatial and temporal average ionization variation (Z*)

Fig. 21(a) represents the spatial variation of the plasma average ionization when the laser power density is 10^{11} W/cm^2 and pulse width is 10 ns. The average ionization begins from 2.1 and increases to reach 3.42 at a distance is about 152 µm. The temporal variation of the plasma average ionization was shown in Fig.21(b). The average ionization begins from 2.45 and stay constant. The spatial variation of the plasma average ionization when the laser power density is 10^{12} W/cm^2 and the pulse width is 10 ns is illustrated in Fig.22(a), The maximum average ionization reaches to 2.5 at about 150 µm. The temporal variation of the plasma average ionization is shown in Fig.22(b), the average ionization will stay at 2.5 until about 4 ns and then increases to reach 11 after 9 ns.

Fig. 23(a) and Fig. 23(b) represent the spatial and temporal variation of the plasma average ionization when the laser power density is 10^{11} W/cm^2 and pulse width is 10 ps. The average ionization has amount similar to that when the laser power density is 10^{12} W/cm^2 and pulse width is 10 ns. The spatial variation of the plasma average ionization when the laser power density is 10^{12} W/cm^2 and pulse width is 10 ps can be shown in Fig.24(a), The average ionization will stay at 2.2 until 155 µm and increases rapidly to reach 3.35. The temporal variation of the plasma average ionization can be explained in Fig.24(b), the average ionization begins from 2.3 and increases to reach 13 after 0.9 ns.

Fig. 25(a) represents the spatial variation of the plasma average ionization when the laser power density is 10^{13} W/cm^2 and pulse width is 10 ps. The maximum average ionization is 13 at 20 µm and stay constant at a long distance. The temporal variation of plasma average ionization Z begins from 3.6 and increases rapidly to reach 13 after 0.8 ns as shown in Fig. 25(b).

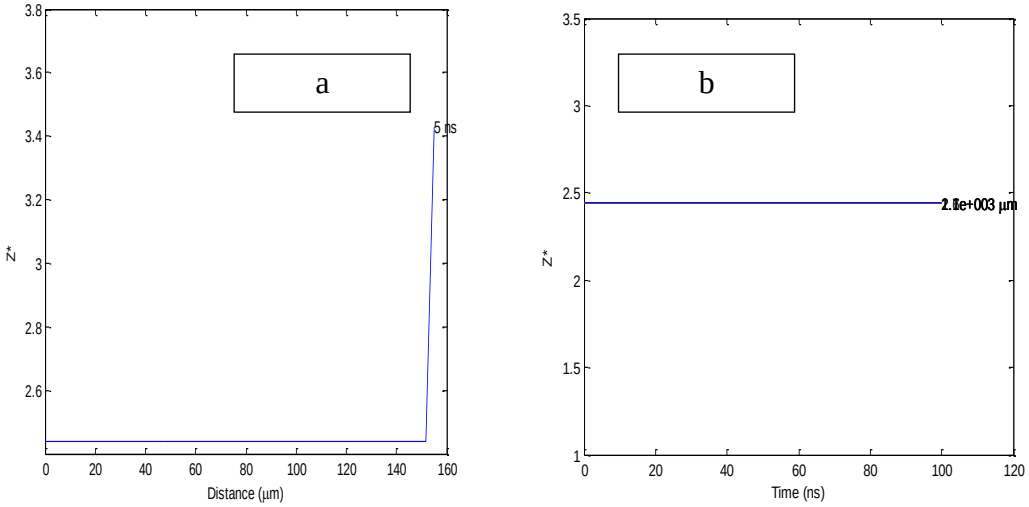

Fig. 21: Spatial and temporal variation of plasma average ionization at intensity 10^{11} W/cm^2 with pulse width 10 ns.

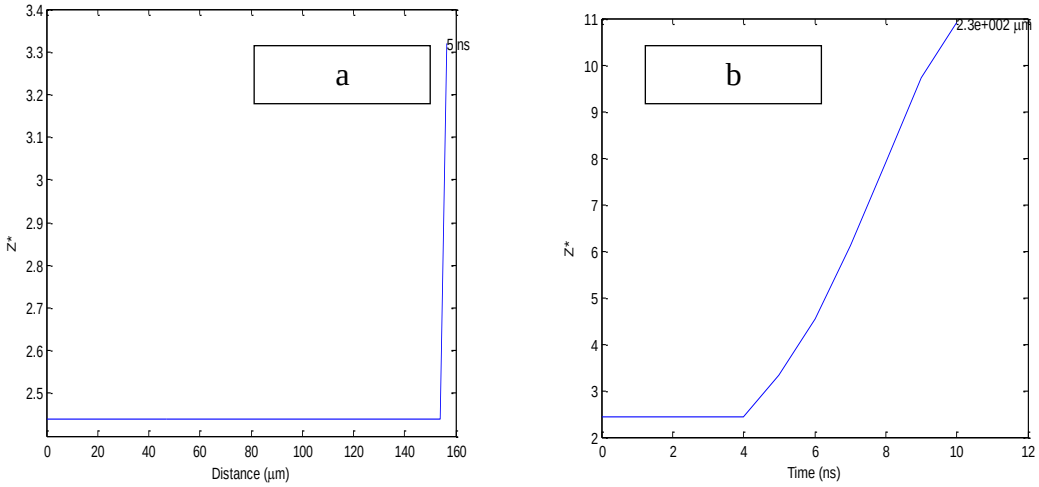

Fig. 22: Spatial and temporal variation of plasma average ionization at intensity 10^{12} W/cm^2 with pulse width 10 ns.

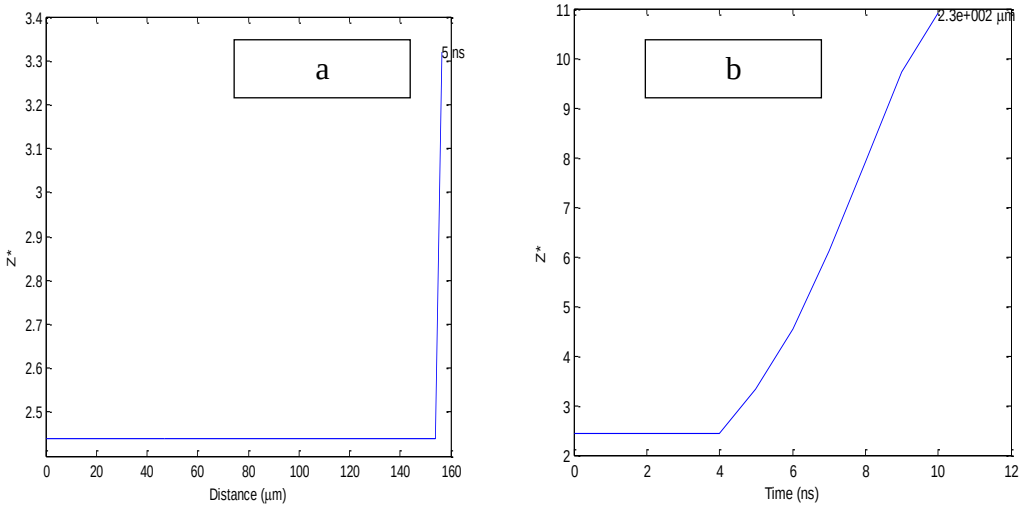

Fig. 23: Spatial and temporal variation of plasma average ionization at intensity 10^{11} W/cm^2 with pulse width 10 ps.

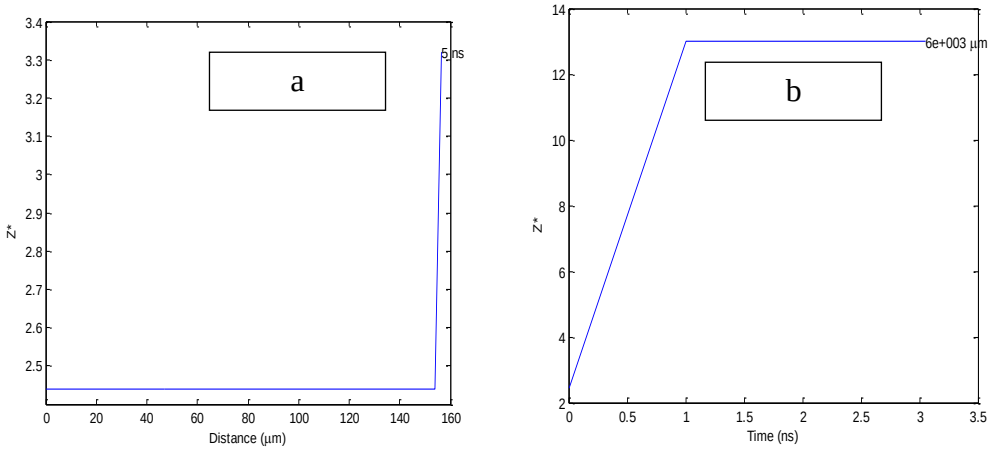

Fig. 24: Spatial and temporal variation of plasma average ionization at intensity 10^{12} W/cm^2 with pulse width 10 ps.

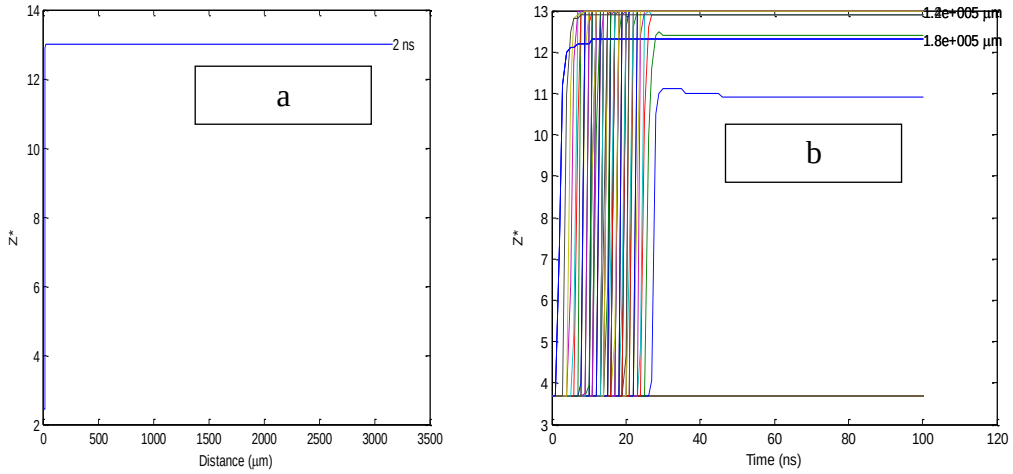

Fig. 25: Spatial and temporal variation of plasma average ionization at intensity 10^{13} W/cm^2 with pulse width 10 ps.

Conclusions

The emission spectrum for aluminum is promising for lithography as it can give 1.82 at 10 nm of the AlV and the emission spectra decreases from this value in the other ionization states of the aluminum. The three laser intensities (10^{11}, 10^{12} and 10^{13} W/cm^2) with the 10 ns laser pulse width for the 1064 nm laser wavelength give high ionization stages for aluminum. The range of average Z obtained from the 1064 nm with 10 ns pulse width is from 2.4-11 for electron temperature range from 16.5-3000 eV. The laser intensity 10^{12} W/cm^2 gives average ionization higher than laser intensity 10^{11} W/cm^2. For the 10 ps laser pulse width and 1064 nm, the average Z range is 3.35-13 while the electron temperature range is from 16.5 to about 2000 eV. The laser pulse width in nanosecond gives more suitable results than pulse width in picosecond. The laser intensity 10^{13}W/cm^2 and pulse width in ps gives average ionization higher than other intensities with the same pulse width.

References

[1] P. Shaaf, "Laser Processing of Material, Springr, New York (2010).
[2] D. R. Corson and P. Lorrain, "Electromagnetic Fields and Waves", Freeman, New York (1988).

[3] S. Eliezer, "The Interaction of High-Power Lasers with Plasmas", Taylor and Francis Inc., U.K. (2002).
[4] R. K. Singh and J. Narayan, Phy. Rev., B41 (1990) 8843-8859.
[5] J. P. Christiansen, D. E. Ashby, K. V. Roberts, Comp. Phys. Commun., 7 (1974) 271-287.
[6] A. R. Bell, "New Equations of State for Medusa", Rutherford Appleton, "New Equations of State for Medusa", Rutherford Appleton Laboratory Report: RL-83-040, RAL, Didcot, U.K, 1983.
[7] A. M. Rodger, A. M. Rogoyski, S. J. Rose, "MED101: A laser- Plasma Simulation Code. User Card", Rutherford Appleton Laboratory Report: RAL-89-127, RAL, Didcot, U. K., 1989.
[8] A. Djaoui, "A user Guide for The Laser Plasma Simulation Code MED103", Rutherford Appleton Laboratory Report: RAL-TR-96-099, RAL, Didcot, U. K., 1996.
[9] R. D. Cowan, L. J. Radziemski,V. Kanfman, J. of The Optical Society of America, 64 (1974) 1474-1477.
[10] I. P. Grant, B. J. Mekenzie, P. H. Norrington, D.F. Mayers, N. C. Pyper, Comp. Phys. Commun., 21 (1980) 207-231.
[11] R. D. Cowan, J. of Optical Society of America, 58 (1968) 808-818.
[12] P. A. Rodgers, A. M. Rogoyski, S. J. Rose, Rutherford Appleton Laboratory Report, RAL-89-127, Dec.1989.
[13] A. Djaoui and A. A. Offenberger, Phys. Rev. E, 50 (1994) 4961-4968.
[14] J. P. Christiansen and K. V. Roberts," OLYMPUS a standard control and utility package for initial-value FORTRAN programs", Comp. Phys. Commun. (1974).
[15] L. Spitzer, Physics of Fully Ionized Gases, 2nd Edition, Inter Science Publishes, (1965).